Scalable mechanochemical amorphization of bimetallic MOF-74 catalyst for selective hydrogenation of CO_2 to methanol

Tomislav Stolar,[†,¶] Anže Prašnikar,[‡,¶] Valentina Martinez,[†] Bahar Karadeniz,[†] Ana Bjelić,[‡] Gregor Mali,[‡] Tomislav Friščić,[†,§] Blaž Likozar,[*,‡] and Krunoslav Užarević[*,†]

†*Ruđer Bošković Institute, Bijenička cesta 54, 10000 Zagreb, Croatia*

‡*National Institute of Chemistry, Hajdrihova 19, SI-1001 Ljubljana, Slovenia*

¶*These authors contributed equally*

§*McGill University, 801 Sherbrooke St. West Montréal, Québec H3A 0B8, Canada*

E-mail: blaz.likozar@ki.si; krunoslav.uzarevic@irb.hr

Keywords: mechanochemistry, ball-milling, MOF-catalyzed methanol production, bimetallic MOF-74, amorphous MOF, CO_2 hydrogenation

Abstract

Selective catalytic reduction of CO_2 to methanol has tremendous importance in the chemical industry. It mitigates two critical issues in modern society, the overwhelming climate change and the dependence on fossil fuels. The most used catalysts are currently based on mixed copper and zinc phases, where the high surface of active copper species is a critical factor for the catalyst performance. Motivated by the recent breakthrough in the controllable synthesis of bimetallic MOF-74 materials by ball milling,

we targeted to study the potential of ZnCu-MOF-74 for catalytic CO_2 reduction. Here, we tested whether the nano-sized channels decorated with readily accessible and homogeneously distributed Zn and Cu metal sites would be advantageous for the catalytic CO_2 reduction. Unlike the inactive monometallic Cu-MOF-74, ZnCu-MOF-74 shows moderate catalytic activity and selectivity for the methanol synthesis. Interestingly, the post-synthetic mechanochemical treatment of desolvated ZnCu-MOF-74 resulted in amorphization and a significant increase in both the activity and selectivity of the catalyst, despite the destruction of the well-ordered and porous MOF-74 architecture. The results emphasize the importance of defects for the MOF catalytic activity, and the potential of amorphous MOFs to be considered as heterogeneous catalysts.

Introduction

Extensive usage of fossil fuels for the production of energy has led to huge amounts of anthropogenic CO_2 emissions. This represents one of the greatest problems facing our society and a pressing need to close the carbon cycle. Therefore, it is of tremendous interest to develop chemical processes that would use carbon dioxide as a feed stock and convert it to useful products. One example of such value-added reaction is catalytic hydrogenation of CO_2, which can non-selectively result in methanol synthesis *via* hydrogenation, CO through reverse-water gas shift (RWGS) reaction, CH_4 through CO_2 methanation or hydrocarbons by a combination of CO_2 reduction with Fischer–Tropsch reactions.[1] Among them, methanol is especially important because it is a bulk commercial chemical and is used as a versatile C_1 source in the chemical industry. If methanol can be efficiently synthesized from atmospheric CO_2, it not only mitigates greenhouse gas emissions but can also be used as a biofuel, hence the origin of the term "methanol economy".[2] One of the most used industrial catalysts for methanol synthesis are the ones based on mixed copper/zinc oxide materials, such as $Cu/ZnO/Al_2O_3$.[3] $Cu/ZnO/Al_2O_3$ (CuZnAl) denotes a family of catalysts comprised of Cu and ZnO nanoparticles, with at least 50 mol% of Cu metal content in the mixture.

The spherical Cu nanoparticles in the industrial catalyst are in a close contact with ZnO nanoparticles. The two types of nanoparticles form aggregates with moderately high surface area of the active Cu nanoparticles. Although the exact role of Cu and ZnO constituents is still debated, a large body of evidence confirms that ZnO dramatically increases the intrinsic activity of the copper catalyst, a phenomenon better known as Cu-ZnO synergy.[3–7] Furthermore, the Al_2O_3 is the most commonly used structural promoter for this catalyst family and leads to increased catalytically active surface area.[8,9]

In constant search for better catalysts, MOFs have garnered special attention due to their unique properties and high catalytic potential stemming from porous architecture and the nature of metal nodes and organic linkers.[10,11] This is particularly emphasized after the recent synthetic breakthroughs enabled the preparation of MOF catalysts containing more than one type of metal node.[12] These multi-metallic MOFs displayed enhanced stability and applicability potential as compared to their monometallic counterparts.[12,13] Particularly interesting class of MOFs in this context is MOF-74,[14] a family of modular MOFs built from various divalent metal cations (M = Zn, Mg, Cu, Ni, Co, Mn, Fe, Cd, and others) and 2,5-dihydroxyterephthalic acid (H_4dhta, Figure 1), widely studied for catalytic and storage applications. The metal cations in MOF-74 form rod-like oxometallic chains along the *c*-crystallographic axis with a complex interactivity among the metal centers and one open coordination site per node for coordination of the guest molecule (Figure 1b right). The oxometallic chains are bridged by fully deprotonated $dhta^{4-}$ to form highly porous honeycomb structure with the channel diameter of approximately 12 Å.[15,16] It was shown recently how the introduction of traces of other metal into the oxometallic chain of MOF-74 will increase the activity and stability of the resulting heterometallic material.[17,18] However, the controllable introduction of specific heterometallic combinations into the oxometallic chains of MOF-74 by conventional procedures still presents a significant challenge.[19] Only recently we demonstrated how ball milling can be used for stoichiometry controlled formation of bimetallic M1M2-MOF-74 with 1:1 M1:M2 molar ratio (Figure 1a).[20] The strategy exploits

different binding capabilities of carboxylic and phenolic functionalities of H_4dhta that allow for the selective and controllable binding of target metals to specific position, affording a series of bimetallic MOF-74 materials with homogeneous distribution of heterometals, high porosity, and stability.

Among other bimetallic MOF-74 materials in the series, we have prepared ZnCu-MOF-74 with 1:1 ratio of Zn and Cu nodes and Brunauer–Emmett–Teller (BET) surface of almost 1000 m^2/g.[20] The Zn and Cu cations are in a close proximity and complex interaction (Figure 1b). In this work, we wanted to establish whether this arrangement, together with a high porosity of ZnCu-MOF-74, could be exploited in the catalytic hydrogenation of CO_2 to methanol. It was recently shown that MOFs can be utilized as support for active nanoparticles (NPs), prevent their aggregation and phase separation, and achieve better selectivity towards methanol synthesis.[5,21–23] Here, we have prepared crystalline ZnCu-MOF-74 (c-ZnCu-MOF-74) and have compared its catalytic performance to monometallic Cu-MOF-74 and the industrial $Cu/ZnO/Al_2O_3$ catalyst. Additionally, we were interested to see whether the introduction of defects and collapse of the porous MOF-74 structure *via* mechanochemical amorphization might play a role in this solid-gas phase heterogeneous catalytic reaction. The results show that, even more than the high porosity and accessibility of Zn and Cu metal nodes, the mechanochemical amorphization has a profound effect both on the catalytic activity and the selectivity of the bimetallic MOF-74 catalyst.

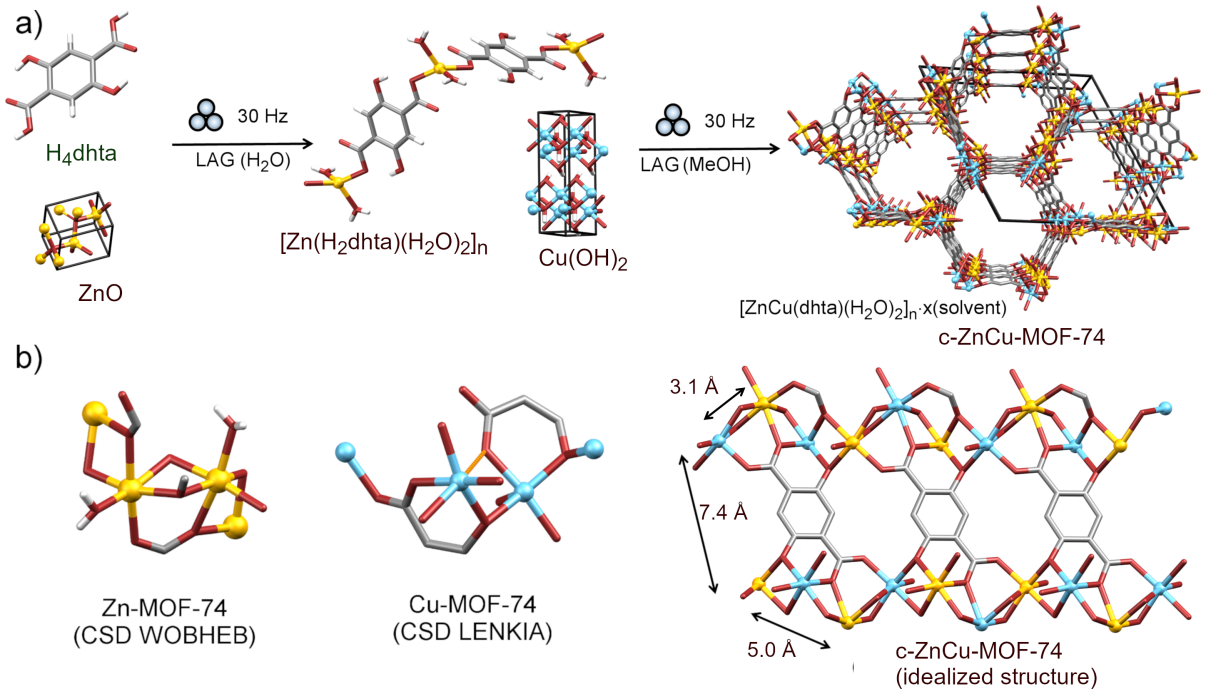

Figure 1: a) Two-step mechanochemical synthesis of bimetallic crystalline ZnCu-MOF-74 (c-Zn-MOF-74) from ZnO and $Cu(OH)_2$; b) cross-sections of Zn-MOF-74 (left), Cu-MOF-74 (center), and idealized ZnCu-MOF-74 (right) walls along the crystallographic *c*-axis. The nearest distances among metal nodes in the oxometallic chain are denoted on the right. CSD denotes the Cambridge Structural Database codes. Color scheme: Zn-yellow, Cu-blue, O-red, C-grey, H-white.

Experimental

Mechanochemical milling reactions where performed using InSolido Technologies IST-500 vibratory ball mill. Reactions were conducted at 30 Hz, in 14 mL PMMA jars and with one 2.7 g tungsten carbide ball as milling media.

Mechanochemical synthesis of c-ZnCu-MOF-74 was carried out in a stepwise manner following recently described procedure (Figure 1).[20] Firstly, 1.5 mmol of ZnO was milled with 1.5 mmol of 2,5-dihydroxyterephtalic acid (H_4dhta) in the presence of 150 μL of H_2O. Liquid assisted grinding (LAG) reaction was conducted for 90 min and after nonporous 2-D [Zn(H_2dhta)(H_2O)$_2$]n coordination polymer was formed,[24] 1.5 mmol of $Cu(OH)_2$ was added together with 250 μL of MeOH. Finally, after 90 more minutes of milling, brown-reddish powder which corresponded to c-ZnCu-MOF-74 was formed, washed three times with a

small volume of MeOH and vacuum-dried. In order to amorphize the crystalline bimetallic MOF and prepare a-ZnCu-MOF-74, c-ZnCu-MOF-74 was held under vacuum at 150 °C overnight to remove the guest and coordinated solvent, after which the sample was milled for 90 min (Figure 2a).[25]

For mechanochemical synthesis of Cu-MOF-74, $Cu(OH)_2$ (292 mg, 3 mmol) and H_4dhta (297 mg, 1.5 mmol) were placed into 14 mL poly(methyl methacrylate) (PMMA) jar along with 400 μL of methanol. The mixture was ground with one 2.7 g WC ball for 30 min at 30 Hz using IST-500 vibratory ball mill (InSolido Technologies). The product was washed three times with 5mL of MeOH then filtered and vacuum dried. Resultant compound was analyzed by PXRD and FTIR-ATR and subjected to the further analyzes described in the main text.

Solid-state ^{13}C magic-angle spinning (MAS) NMR spectra were recorded on a 600 MHz Varian VNMRS spectrometer equipped with 1.6 mm HXY Varian MAS probe. MAS frequencies ranged between 32 kHz and 40 kHz. The spectra of copper-containing samples were obtained with Hahn echo sequence. Duration of 90- and 180-degree pulse was 2 μs and 4 μs, respectively, and the inter-pulse delay was equal to one rotation period. Repetition delay between consecutive scans was 100 ms and the number of scans was 800 000. ^{1}H–^{13}C cross-polarization (CP) MAS NMR spectrum of Zn-MOF-74 was recorded at MAS frequency of 32 kHz using a ramp during 5 ms CP block and high-power XiX proton decoupling during acquisition. Repetition delay was 2 s and number of scans was 3200. All ^{13}C shifts are reported relative to the position of the ^{13}C signal of tetramethylsilane (TMS).

Scanning electron microscopy (SEM) was performed on SUPRA35 VP(Carl Zeiss) coupled with EDS detector Inca 400 (Oxford Instruments). The samples were coated by 3 nm of Au using calibrated Precision Etching and Coating System, Gatan 682.

N_2 physisorption was used to obtain specific surface areas and other parameters. Measurements were performed on Micromeritics ASAP 2020, with the degassing at 150 °C for 20 h with 50 mg of sample. BET surface area and pore volume were determined using

adsorption data.

Catalytic tests were performed in a parallel reactor system with online gas composition analysis using gas chromatography (Agilent 490 Micro GC, TCD detectors equipped with CP-Molsieve and PoraPlot U columns). Gas mixture with ratio H_2/CO_2=3 was prepared by mixing H_2 (99.999%, Messer) and CO_2 (99.999%, Messer). Samples (200 mg) were mixed with SiC (1 g, 300 μm) to ensure sufficient thermal conductivity and uniform gas flow. Mixtures were then inserted into packed bed reactors and prereduced at 230 °C for 12 h in pure H_2 at 1 bar. The catalytic tests were performed between 160-230 °C, 20 bar and flow 33,000 NmL/g_{cat}h. Commercial CuZnAl catalyst HiFuel W230 (particle sizes 240-400 μm) was used as a reference for methanol synthesis.

Results and discussion

Mechanochemistry, i.e., chemical reactivity in the solid state induced by mechanical action,[26,27] emerged recently as a sustainable method for the rapid and green production[24,28] of several functional MOFs.[29–32] These mechanochemical procedures were developed without using bulk solvents, and are applicable even in a continuous production on pilot scales using a twin-screw extrusion.[33,34] Moreover, the mechanochemical procedures offer a unique level of selectivity and control. An efficient mechanochemical preparation of bimetallic MOFs is demonstrated by either: (a) milling together already synthesized MOFs in a mechanochemical alloying approach,[35,36] or (b) using a bottom-up approach where bimetallic MOFs are synthesized in a stepwise manner starting from inorganic sources and organic ligands thus gaining a control over the metals stoichiometric ratio and minimizing solvent consumption.[20]

As evidenced from Figure 2a, a-ZnCu-MOF-74 lacks long-range crystal ordering and exhibits a broad PXRD pattern absent of characteristic Bragg peaks. FTIR spectra of c-ZnCu-MOF-74 shows sharp signals that broaden and shift upon amorphization. However, the most notable difference is the appearance of a new band at 1727 cm^{-}1 which is assigned to the

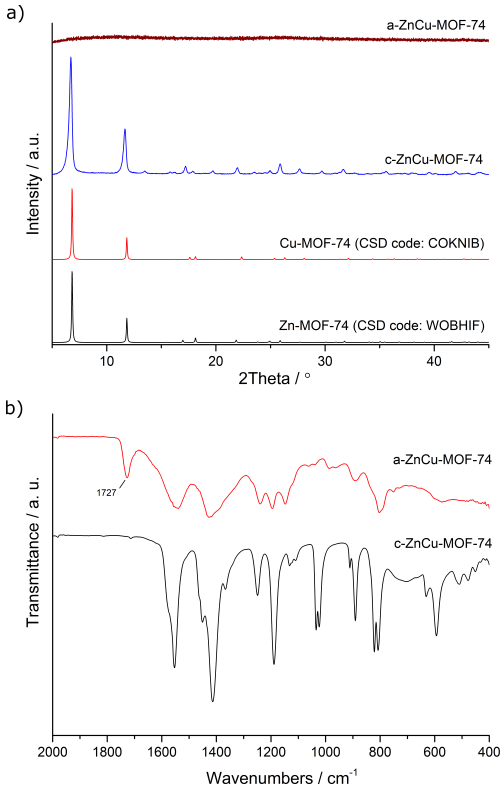

Figure 2: a) PXRD patterns of mechanochemically synthesized c-ZnCu-MOF-74 and a-ZnCu-MOF-74 compared to monometallic Zn-MOF-74 and Cu-MOF-74; b) FTIR spectra of mechanochemically synthesized c-ZnCu-MOF-74 and a-ZnCu-MOF-74. New band that appears in a-ZnCu-MOF-74 at 1727 cm^{-1} is highlighted.

stretching vibration of uncoordinated carbonyl group. This suggests that the amorphization proceeds *via* partial breakage of the node-linker carboxylate bonds, thus creating a defective coordination spheres around copper and zinc nodes. The recent theoretical study has shown that the linker-metal bonds in MOF-74 materials are dynamic and can brake under certain conditions.[37] Similar observations of the appearance of uncoordinated carbonyl group were also recently described in the case of mechanochemical amorphization of Ni-MOF-74, where the amorphization led to spin-crossover and significant drop in magnetization.[25] Furthermore, there seems to be a correlation between the mechanochemical amorphization and the introduction of defects as observed by Bennett *et al.* in zirconia-based MOFs.[38]

The established BET surface area of the here prepared bimetallic c-ZnCu-MOF-74 is about 660 m^2/g, which is slightly lower than the reference (910 m^2/g).[20] There is a large

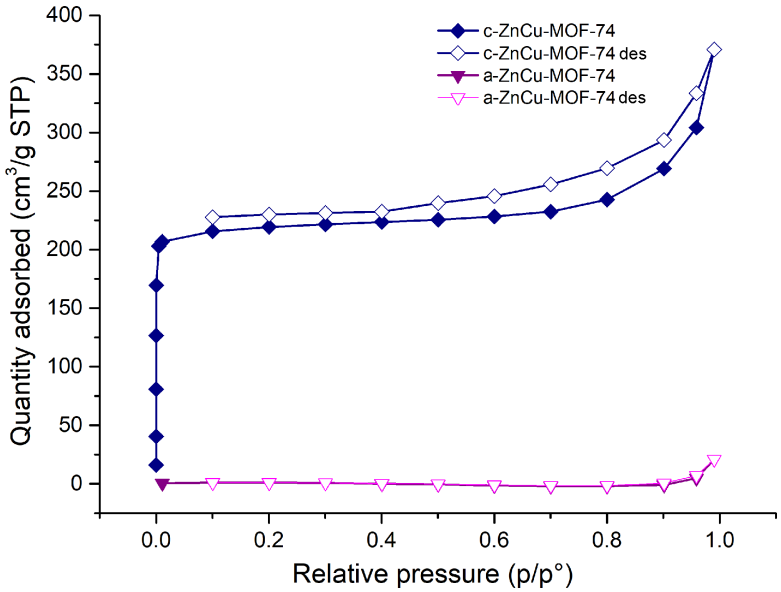

Figure 3: Nitrogen adsorption-desorption isotherms measured at 77K for crystalline and amorphous ZnCu-MOF-74 catalysts prepared by mechanochemical processing.

difference in porosity between the crystalline and amorphous samples (Figure 3). The surface area of a-ZnCu-MOF-74 is 250-times lower than surface area of c-ZnCu-MOF-74 (2.6 m^2/g). Also, the pore volume of materials drops from 0.56 cm^3/g in c-ZnCu-MOF-74 to 0.029 cm^3/g after the mechanochemical treatment. Mechanochemical incorporation of defects to activated c-ZnCu-MOF-74 thus leads to the fast collapse of the open and porous MOF-74 structure, as was already observed for Ni- and Zn-MOF-74.[25]

The difference in guest accommodation properties for two materials is also visible from thermogravimetric analysis (TGA). The initial mass loss in c-ZnCu-MOF-74 starts almost immediately upon heating, denoting the loss of MeOH and water guests from the channels (Figures S7 and S8). Amorphous a-ZnCu-MOF-74 exhibits a less pronounced step in the same temperature region, due to the presence of a limited amount of guests in the collapsed MOF structure. Both materials show similar decomposition profiles in the range of 400-900 °C, indicating that the collapse of the long-range ordering had little effect on the thermal stability of ZnCu-MOF-74 materials.

In order to probe local ordering of metals in c-ZnCu-MOF-74 and a-ZnCu-MOF-74 solid catalysts, we utilized solid-state nuclear magnetic resonance spectroscopy (ssNMR).[39,40] As

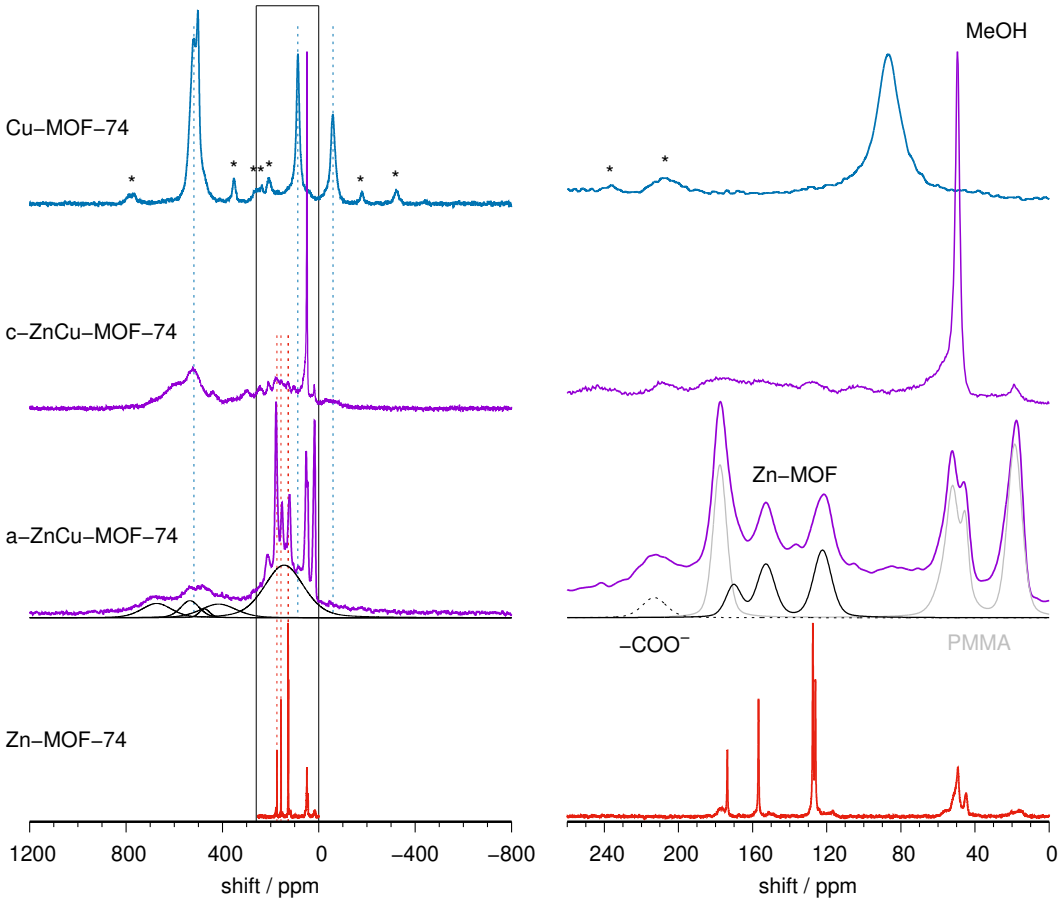

Figure 4: ^{13}C MAS NMR spectra of c-ZnCu-MOF-74 and a-ZnCu-MOF-74, compared to the corresponding spectra of the crystalline Zn-MOF-74 and Cu-MOF-74. Left panel shows full spectra; asterisks above the spectrum of Cu-MOF-74 mark the spinning sidebands; in the spectrum of a-ZnCu-MOF-74 individual broad contributions, as identified by the spectral deconvolution, are shown by black solid lines; red and blue vertical dotted lines mark the positions of the ^{13}C signals of Zn-MOF-74 and Cu-MOF-74, respectively. Right panel shows only a selected part of the spectra; contributions of MeOH, Zn-MOF-74 domains, PMMA impurities, and potential -COO$^-$ groups are denoted.

evident from Figure 4, neither the ^{13}C MAS NMR spectrum of c-ZnCu-MOF-74 nor the spectrum of a-ZnCu-MOF-74 is a simple sum of the spectra of Zn-MOF-74 and Cu-MOF-74. This indicates that the two bimetallic samples are not mixtures of two single-metal phases and are not composed only of single-metal domains. The ^{13}C MAS NMR spectra of c-ZnCu-MOF-74 and a-ZnCu-MOF-74 are rather similar, but not identical one to another. They both exhibit several narrow signals in the range between 0 and 240 ppm, and several broad signals in the range between 0 and 800 ppm. The narrow signals belong to carbon atoms in diamagnetic amorphous species. In the spectrum of a-ZnCu-MOF-74 the signals at 18, 45, 52, and 178 ppm belong to PMMA, an impurity introduced by milling, whereas the signals at 123, 155 and 170 ppm belong to domains of amorphous ZnCu-MOF-74. There is an additional narrow signal present at about 213 ppm, which might correspond to the unbound and deprotonated -COO^- groups of the linker molecules. The broad signals belong to carbon atoms, which are close to paramagnetic Cu centres. Strong hyperfine coupling among the unpaired electronic spins of copper ions and nuclear spins of ^{13}C nuclei gives rise to huge shifts and broadening of these signals. The number, the positions and the widths of the broad signals of c-ZnCu-MOF-74 and a-ZnCu-MOF-74 are different from those in the spectrum of the pure crystalline Cu-MOF-74. This strongly suggests that Zn and Cu atoms are partially well dispersed and 'intimately' mixed within the two mixed-metal frameworks, giving rise to a number of different chemical environments for the nearby carbon atoms. As already mentioned, ^{13}C MAS NMR spectra of c-ZnCu-MOF-74 and a-ZnCu-MOF-74 are somewhat different one from another. In the spectrum of the crystalline material we can notice a strong, sharp signal of MeOH, which is not present in the spectrum of the amorphous material. More interestingly, the spectra of the two bimetallic samples exhibit differences also in the broad signals resonating in the range between 300 and 800 ppm; these complies with the results of the IR analysis indicating that the connectivity of Zn and Cu within the frameworks of the crystalline and amorphous ZnCu-MOF-74 are somewhat different.

Mechanochemical synthesis afforded the c-ZnCu-MOF-74 material particles with irreg-

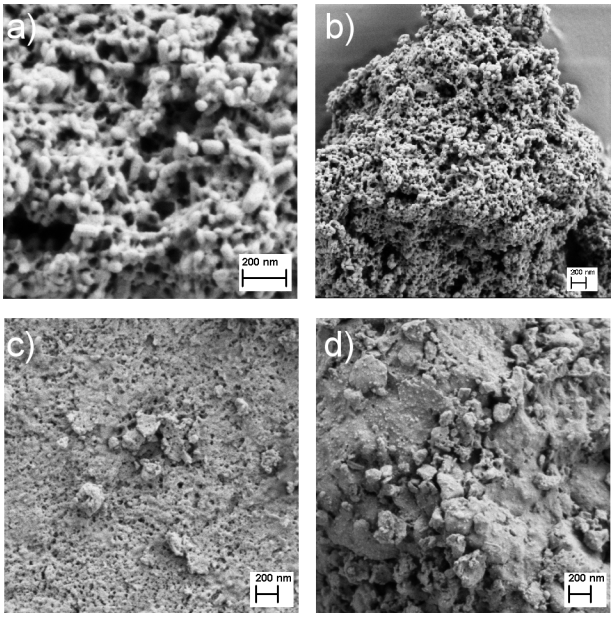

Figure 5: a) SEM micrographs for a) and b) crystalline ZnCu-MOF-74; c) amorphous ZnCu-MOF-74; and d) amorphous ZnCu-MOF-74 after catalysis.

ular shape and a broad size ranging from 10 to 80 nm (Figures 5a and b). Based on the performed SEM-EDS analysis, both the crystalline and amorphous ZnCu-MOF-74 materials have homogeneous distribution and similar loading of copper and zinc metals on the surface (Figures S9-S11). The crystalline sample exhibits hierarchical structure of separated porous MOF particles thus showing potential for excellent gas transport properties. On the other hand, amorphization changes catalyst morphology and the a-ZnCu-MOF-74 material consists of smaller particles of average size of 5-30 nm, which are dispersed without much agglomeration (Figure 5c). This arrangement may assist in allowing the direct access of gases to Cu- and Zn-based phases on the catalyst surface. After the catalytic process, the amorphous particles form conglomerates with diameter of 50-200 nm, again consisted of nano-sized MOF particles (Figure 5d).

During CO_2 reduction using MOF samples, we observed a formation of H_2O, CO and MeOH. Compared to the monometallic Cu-MOF-74 catalyst, the activity toward MeOH synthesis increased by 4-6 times when using the bimetallic c-ZnCu-MOF-74 (Figure 6). It is already established that zinc increases the binding energy of the reaction intermediates

on Cu surface in commercial catalysts, causing a formation of more active catalytic sites by lowering activation energy of critical elementary steps toward MeOH.[3] One important factor for the activity of commercial CuZnAl catalyst is the high surface area of active copper species achieved by dispersion in ZnO/Al_2O_3 matrix. We expected here the crystalline and highly-porous c-ZnCu-MOF-74 to readily compete with the commercial CuZnAl catalyst. However, the observed catalytic methanol production rise further when using amorphous a-ZnCu-MOF-74, with collapsed structure and very low porosity (Figure 6). The activity of a-ZnCu-MOF-74 even increases during catalytic test at 230 °C. MeOH molar fraction increased in 2 hours by 1, 5 and 21% for Cu, c-ZnCu and a-ZnCu(-MOF-74) at 230 °C respectively. Large increase of the MeOH synthesis rate with a-ZnCu-MOF-74 is highly likely due to the lack of rigid structure, active metal sites on disordered MOF surfaces, and the sintering of Cu particles, which all cause MeOH TOF increase.[41,42] Change of the reaction rate was much lower when catalytic tests were repeated by lowering temperature down to 160 °C (Figure 6). Overall, the c-ZnCu-MOF-74 sample activity increased by 4-7 fold after amorphization. The surface area of a-ZnCu-MOF-74 is about 250-times lower than the one of the crystalline sample which points to the fact that, for this industrial setup, the introduction of defects in the MOF catalyst enables the creation of more active sites for MeOH synthesis and plays more important role than the well-ordered and porous MOF architecture. The PXRD analysis of the catalyst after the catalytic cycle reveal traces of copper nanoparticles in amorphous matrix (Figure S12).

The impact of the catalyst structure and composition on the catalytic properties was examined using Arrhenius plot (Figure 7). The concentration of MeOH and CO of the last four stable points at single temperature step were averaged and plotted. The CO concentration below 10^{-3} % could not be determined due to experimental limitations. The apparent activation energies (E_A) were determined at temperatures below 200 °C to avoid mistakes due to the possible mass transfer limitation or proximity to equilibrium. Due to the high gas flow rate (WHSV=33.000 $NmL/g_{cat}h$) the CO_2 conversion at the highest conversion of

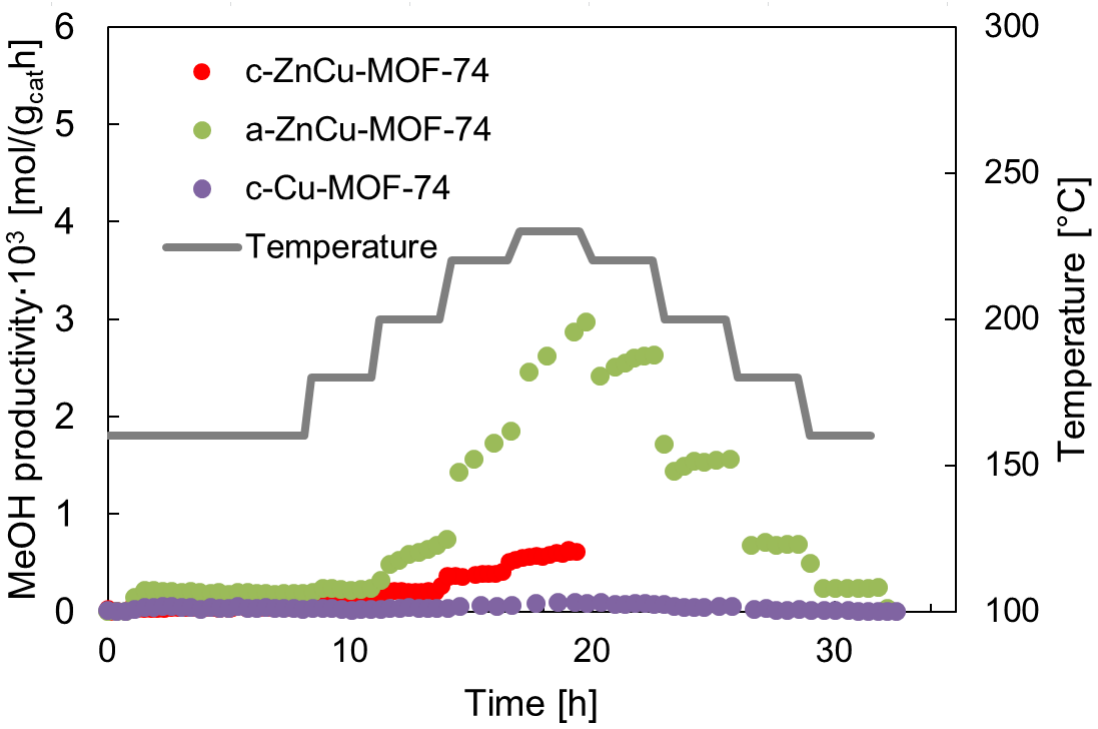

Figure 6: The evolution of MeOH molar productivity during the catalytic experiments.

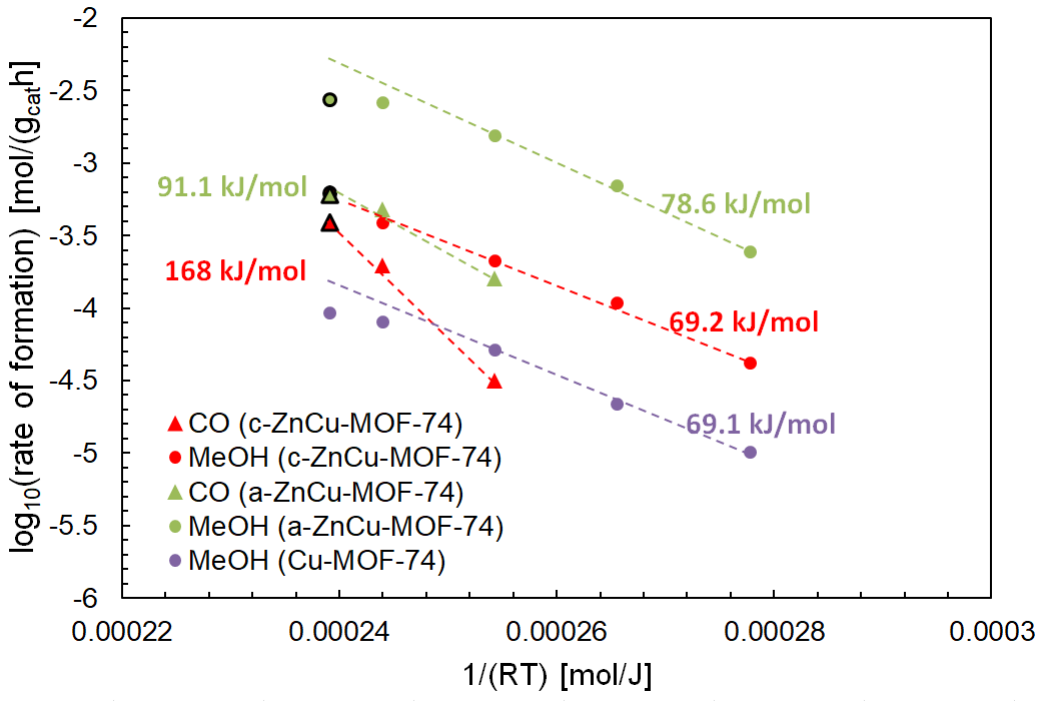

Figure 7: Comparison of the catalytic activities of different MOFs. E_A are determined in low temperature range to avoid apparent decrease of E_A due to reaction proximity to chemical equilibrium. The circled points with black line indicates points that did not reach steady state.

MOF are low (0.9% for a-ZnCu-MOF-74). Therefore, the decrease of the MeOH productivity due to the proximity to the chemical equilibrium at high temperature is not expected. It is observed that at higher temperatures the log of rate of MeOH formation for a-ZnCu-MOF-74 and Cu-MOF-74 deviates from linear Arrhenius correlation, indicating intraparticle mass transfer limitation.[43,44] Artificial linear correlation at T>200 °C is observed for c-ZnCu-MOF-74, because the data points obtained are from the part of the catalytic tests where temperature is increased, causing morphology change and increased activity. The apparent activation energy and preexponential factor of CO_2 to CO reaction (RWGS) are much higher for c-ZnCu-MOF-74 in comparison to a-ZnCu-MOF-74 catalyst, pointing to a large difference in the reaction mechanism. The rate of competitive RWGS reaction of crystalline sample increases nearly up to the rate of MeOH synthesis at 230 °C.

Table 1: The values of E_A, A and r parameters for MeOH and CO formation at 200 °C.

	MeOH			CO		
Sample	Ea*	log(A)**	r(200 °C)**	Ea*	log(A)**	r(200 °C)**
a-ZnCu-MOF-74	78.6	5.9	$1.6 \cdot 10^{-3}$	91.1	6.3	$1.1 \cdot 10^{-4}$
c-ZnCu-MOF-74	69.2	4.0	$2.2 \cdot 10^{-4}$	168	14.0	$3.2 \cdot 10^{-5}$
c-Cu-MOF-74	69.1	3.3	$5.0 \cdot 10^{-5}$	na	na	na
CuZnAl	62.8	4.8	$7.4 \cdot 10^{-3}$	149	13.8	$2.0 \cdot 10^{-3}$

*unit kJ/mol, ** unit mol/(g_{cat}h)

The Table 1 contains E_A, pre-exponential factors A and the rates of MeOH and CO synthesis (r), including comparison with commercial CuZnAl catalyst. It is observed that the activation energy for methanol synthesis catalyzed by MOF samples is similar to the one when using CuZnAl catalyst. The catalytic properties for CO formation of a-ZnCu-MOF-74 sample are very special with a large difference in the value of apparent activation energy (91.1 kJ/mol) comparing to the CuZnAl sample (149 kJ/mol). This could occur due to a difference in the exposure of terminal crystal plane of Cu, since apparent energy for CO formation varies from 78 kJ/mol on Cu(110) to 135 kJ/mol on polycrystalline Cu, while it is significantly more constant for MeOH synthesis where it varies between 67 and 77 kJ/mol for Cu(110) and polycrystalline Cu respectively.[45]

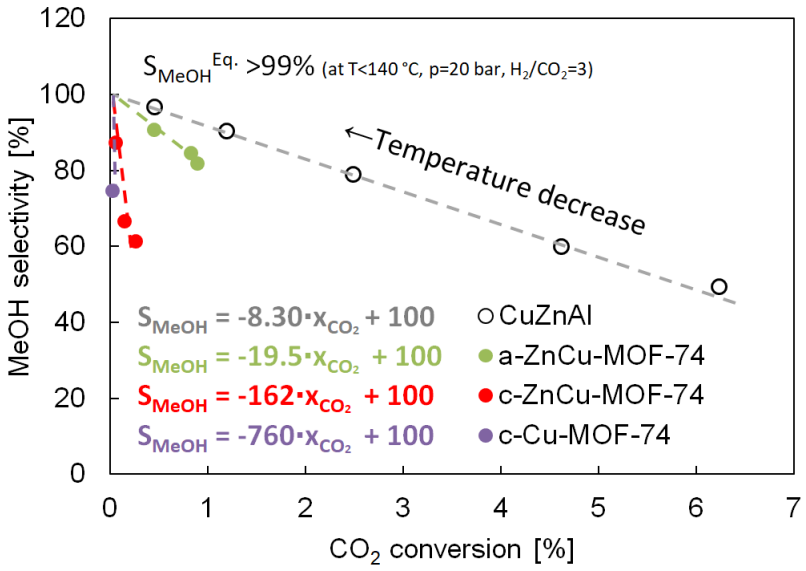

Figure 8: MeOH selectivity (S_{MeOH}) at the same CO_2 conversion (x_{CO_2}) increases in order: Cu-MOF-74<c-ZnCu-MOF-74<a-ZnCu-MOF-74<CuZnAl. Commercial CuZnAl catalyst is, as expected, objectively more selective at certain catalyst activity. a-ZnCu-MOF-74 displays significantly higher selectivity than crystalline c-ZnCu-MOF-74. MeOH selectivity converges to 100% at zero CO_2 conversion as expected by chemical equilibrium by decreasing temperature below 140 °C as determined using Gaseq.[46]

The selectivity toward MeOH therefore increases by defects introducing into the bimetallic MOF structure (Figure 8), allowing copper phase agglomeration, which is also in line with the conclusions about the basis for activity of the industrial CuZnAl catalyst. The performance enhancing parameters in CuZnAl system are presence of the Cu surface plane steps by increasing Cu particle size[41,42] and strong metal-support interaction (SMSI) which enables high degree of Cu substitution with Zn atoms and consequently favorable binding of reaction intermediates.[3,47] Addition of Zn to the c-Cu-MOF-74 increases MeOH synthesis selectivity by 4.7 times which is a consequence of incorporation of Zn into the active Cu phase. The amorphization of c-ZnCu-MOF-74 decreases the surface area, but also reduces the particle sizes and change the coordination sphere of the metal nodes in MOF-74, thus increasing the MeOH selectivity by a factor of 8.3. Separated Cu atoms or small Cu clusters in crystalline MOF tend to promote competitive reverse water gas shift reaction, while the amorphization leads to the promotion of methanol synthesis.

Conclusion

To summarize, unlike the monometallic Cu-MOF-74, bimetallic crystalline ZnCu-MOF-74 prepared by mechanochemical procedure shows activity for the catalytic reduction of CO_2 to methanol. Mechanochemical treatment of the activated and degassed crystalline ZnCu-MOF-74 results in the formation of amorphous and non-porous a-ZnCu-MOF-74 with similar distribution of heterometal nodes as in the crystalline phase. The spectroscopic analyses show that the coordination sphere of the nodes is changed upon amorphization, most likely due to breaking of carboxylate-metal bonds. The catalyst activity is significantly higher for the amorphous ZnCu-MOF-74 than the crystalline counterpart due to the additional active sites formed during the amorphization. More importantly, the selectivity of process changes upon amorphization of the c-ZnCu-MOF-74. In reaction catalyzed by amorphous ZnCu-MOF-74 the selectivity towards methanol formation is comparable even to the industrial $Cu/ZnO/Al_2O_3$ benchmark. For the methanol synthesis reaction, the introduction of defects *via* amorphization thus seems to be more important than the catalyst porosity, revealing that the CO_2 reduction is conducted on the surface of the MOF catalyst. Our future work will be directed towards exploiting the potential of mechanochemical MOF transformations[28] for expanding the portfolio of catalytically active non-conventional MOF materials.

Acknowledgement

Tomislav Stolar acknowledges EIT Climate-KIC Alumni for the micro-grant award. Tomislav Friščić acknowledges the support of McGill University William J. Dawson Scholarship. Anže Prašnikar and Blaž Likozar acknowledge Slovenian Research Agency (research core funding No. P2-0152) and Project FReSMe No. 727504. Gregor Mali acknowledges the financial support by the Slovenian Research Agency (research core funding No. P1-0021 and project No. N1-0079). The work has been supported in part by the "Research Cooperability" Program of the Croatian Science Foundation funded by the European Union from the European

Social Fund under the Operational Program Efficient Human Resources 2014-2020, through grant PZS-2019-02-4129. The authors acknowledge networking support by the COST Action CA18112 - Mechanochemistry for Sustainable Industry (www.mechsustind.eu) supported by COST (European Cooperation in Science and Technology, www.cost.eu).

Supporting Information Available

Characterization data (PXRD, IR, DSC, TGA, and SEM) for all new compounds.

Conflict of Interest

Krunoslav Užarević is a share-holder in InSolido Technologies.

References

(1) Porosoff, M. D.; Yan, B.; Chen, J. G. Catalytic reduction of CO_2 by H_2 for synthesis of CO, methanol and hydrocarbons: challenges and opportunities. *Energy Environ. Sci* **2016**, *9*, 62–73.

(2) Goeppert, A.; Czaun, M.; Jones, J.-P.; Surya Prakash, G. K.; Olah, G. A. Recycling of carbon dioxide to methanol and derived products – closing the loop. *Chem. Soc. Rev.* **2014**, *43*, 7995–8048.

(3) Behrens, M.; Studt, F.; Kasatkin, I.; Kühl, S.; Hävecker, M.; Abild-Pedersen, F.; Zander, S.; Girgsdies, F.; Kurr, P.; Kniep, B.-L.; Tovar, M.; Fischer, R. W.; Nørskov, J. K.; Schlögl, R. The Active Site of Methanol Synthesis over $Cu/ZnO/Al_2O_3$ Industrial Catalysts. *Science* **2012**, *336*, 893–898.

(4) Huš, M.; Dasireddy, V. D. B. C.; Štefančič, N. S.; Likozar, B. Mechanism, kinetics

and thermodynamics of carbon dioxide hydrogenation to methanol on $Cu/ZnAl_2O_4$ spinel-type heterogeneous catalysts. *Appl. Catal. B* **2017**, *207*, 267–278.

(5) An, B.; Zhang, J.; Cheng, K.; Ji, P.; Wang, C.; Lin, W. Confinement of Ultrasmall Cu/ZnOx Nanoparticles in Metal-Organic Frameworks for Selective Methanol Synthesis from Catalytic Hydrogenation of CO_2. *J. Am. Chem. Soc* **2017**, *139*, 3834–3840.

(6) Huš, M.; Kopač, D.; Likozar, B. Catalytic Hydrogenation of Carbon Dioxide to Methanol: Synergistic Effect of Bifunctional Cu/perovskite Catalysts. *ACS Catal.* **2019**, *9*, 105–116.

(7) Gaikwad, R.; Reymond, H.; Phongprueksathat, N.; Rudolf von Rohr, P.; Urakawa, A. From CO or CO_2?: space-resolved insights into high-pressure CO_2 hydrogenation to methanol over $Cu/ZnO/Al_2O_3$. *Catal. Sci. Technol.* **2020**, *10*, 2763–2768.

(8) Kurtz, M.; Wilmer, H.; Genger, T.; Hinrichsen, O.; Muhler, M. Deactivation of Supported Copper Catalysts for Methanol Synthesis. *Catal. Lett.* **2003**, *86*, 77–80.

(9) Prašnikar, A.; Pavlišič, A.; Ruiz-Zepeda, F.; Kovač, J.; Likozar, B. Mechanisms of Copper-Based Catalyst Deactivation during CO_2 Reduction to Methanol. *Ind. Eng. Chem. Res* **2019**, *58*, 13021–13029.

(10) Gascon, J.; Corma, A.; Kapteijn, F.; Llabrés, F. X. Metal Organic Framework Catalysis: Quo vadis? *ACS Catal.* **2014**, *4*, 361–378.

(11) Yang, D.; Gates, B. C. Catalysis by Metal Organic Frameworks: Perspective and Suggestions for Future Research. *ACS Catal.* **2019**, *9*, 1779–1798.

(12) Chen, L.; Wang, H.-F.; Li, C.; Xu, Q. Bimetallic metal–organic frameworks and their derivatives. *Chem. Sci.* **2020**, *11*, 5369–5403.

(13) Abednatanzi, S.; Derakhshandeh, P. G.; Depauw, H.; Coudert, F. X.; Vrielinck, H.;

Voort, P. V. D.; Leus, K. Mixed-metal metal–organic frameworks. *Chem. Soc. Rev.* **2019**, *48*, 2535–2565.

(14) Rosi, N. L.; Kim, J.; Eddaoudi, M.; Chen, B.; O'Keeffe, M.; Yaghi, O. M. Rod Packings and Metal-Organic Frameworks Constructed from Rod-Shaped Secondary Building Units. *J. Am. Chem. Soc* **2005**, *127*, 1504–1518.

(15) Dietzel, P. D. C.; Panella, B.; Hirscher, M.; Blom, R.; Fjellvåg, H. Hydrogen adsorption in a nickel based coordination polymer with open metal sites in the cylindrical cavities of the desolvated framework. *Chem. Commun.* **2006**, 959–961.

(16) Rowsell, J. L. C.; Yaghi, O. M. Effects of Functionalization, Catenation, and Variation of the Metal Oxide and Organic Linking Units on the Low-Pressure Hydrogen Adsorption Properties of Metal-Organic Frameworks. *J. Am. Chem. Soc* **2006**, *128*, 1304–1315.

(17) Botas, J. A.; Calleja, G.; Sánchez-Sánchez, M.; Orcajo, M. G. Effect of Zn/Co ratio in MOF-74 type materials containing exposed metal sites on their hydrogen adsorption behaviour and on their band gap energy. *Int. J. Hydrog. Energy* **2011**, *36*, 10834–10844.

(18) Jiao, Y.; Morelock, C. R.; Burtch, N. C.; Mounfield, W. P.; Hungerford, J. T.; Walton, K. S. Tuning the Kinetic Water Stability and Adsorption Interactions of Mg-MOF-74 by Partial Substitution with Co or Ni. *Ind. Eng. Chem. Res* **2015**, *54*, 12408–12414.

(19) Wang, L. J.; Deng, H.; Furukawa, H.; GÃ¡ndara, F.; Cordova, K. E.; Peri, D.; Yaghi, O. M. Synthesis and Characterization of Metal-Organic Framework-74 Containing 2, 4, 6, 8, and 10 Different Metals. *Inorg. Chem* **2014**, *53*, 5881–5883.

(20) Ayoub, G.; Karadeniz, B.; Howarth, A. J.; Farha, O. K.; Dilović, I.; Germann, L. S.; Dinnebier, R. E.; Užarević, K.; Friščić, T. Rational Synthesis of Mixed-Metal Microporous Metal-Organic Frameworks with Controlled Composition Using Mechanochemistry. *Chem. Mater.* **2019**, *31*, 5494–5501.

(21) Rungtaweevoranit, B.; Baek, J.; Araujo, J. R.; Archanjo, S.; Choi, K. M.; Yaghi, O. M.; Somorjai, G. A. Copper Nanocrystals Encapsulated in Zr-based Metal-Organic Frameworks for Highly Selective CO_2 Hydrogenation to Methanol. *Nano Lett.* **2016**, *16*, 7645–7649.

(22) Kobayashi, H.; Taylor, J. M.; Mitsuka, Y.; Ogiwara, N.; Yamamoto, T.; Toriyama, T.; Matsumura, S.; Kitagawa, H. Charge transfer dependence on CO_2 hydrogenation activity to methanol in Cu nanoparticles covered with metal–organic framework systems. *Chem. Sci.* **2019**, *10*, 3289–3294.

(23) Gutterød, E. S.; Lazzarini, A.; Fjermestad, T.; Kaur, G.; Manzoli, M.; Bordiga, S.; Svelle, S.; Lillerud, K. P.; Skúlason, E.; Øien Ødegaard, S.; Nova, A.; Olsbye, U. Hydrogenation of CO2 to Methanol by Pt Nanoparticles Encapsulated in UiO-67: Deciphering the Role of the Metal–Organic Framework. *J. Am. Chem. Soc* **2020**, *142*, 999–1009.

(24) Julien, P. A.; Motillo, C.; Friščić, T. Metal–organic frameworks meet scalable and sustainable synthesis. *Green Chem.* **2017**, *19*, 2729–2747.

(25) Muratović, S.; Karadeniz, B.; Stolar, T.; Lukin, S.; Halasz, I.; Herak, M.; Mali, G.; Krupskaya, Y.; Kataev, V.; Žilić, D.; Užarević, K. Impact of dehydration and mechanical amorphization on the magnetic properties of Ni(II)-MOF-74. *J. Mater. Chem. C* **2020**, *8*, 7132–7142.

(26) James, S. L.; Adams, C. J.; Bolm, C.; Braga, D.; Collier, P.; Friščić, T.; Grepioni, F.; Harris, K. D. M.; Hyett, G.; Jones, W.; Krebs, A.; Mack, J.; Maini, L.; Orpen, A. G.; Parkin, I. P.; Shearouse, W. C.; Steed, J. W.; Waddell, D. C. Mechanochemistry: opportunities for new and cleaner synthesis. *Chem. Soc. Rev.* **2012**, *41*, 413–447.

(27) Do, J.-L.; Friščić, T. Chemistry 2.0: Developing a New, Solvent-Free System of Chemical Synthesis Based on Mechanochemistry. *Synlett* **2017**, *28*, 2066–2092.

(28) Stolar, T.; Užarević, K. Mechanochemistry: an efficient and versatile toolbox for synthesis, transformation, and functionalization of porous metal–organic frameworks. *CrystEngComm* **2020**, *22*, 4511–4525.

(29) Pichon, A.; James, S. L. An array-based study of reactivity under solvent-free mechanochemical conditions—insights and trends. *CrystEngComm* **2008**, *10*, 1839.

(30) Beldon, P. J.; Fábián, L.; Stein, R. S.; Thirumurugan, A.; Cheetham, A. K.; Friščić, T. Rapid Room-Temperature Synthesis of Zeolitic Imidazolate Frameworks by Using Mechanochemistry. *Angew. Chem. Int. Ed.* **2010**, *49*, 9640–9643.

(31) Julien, P. A.; Užarević, K.; Katsenis, A. D.; Kimber, S. A. J.; Wang, T.; Farha, O. K.; Zhang, Y.; Casaban, J.; Germann, L. S.; Etter, M.; Dinnebier, R. E.; James, S. L.; Halasz, I.; Friščić, T. In Situ Monitoring and Mechanism of the Mechanochemical Formation of a Microporous MOF-74 Framework. *J. Am. Chem. Soc.* **2016**, *138*, 2929–2932.

(32) Užarević, K.; Wang, T. C.; Moon, S.-Y.; Fidelli, A. M.; Hupp, J. T.; Farha, O. K.; Friščić, T. Mechanochemical and solvent-free assembly of zirconium-based metal–organic frameworks. *Chem. Commun.* **2016**, *52*, 2133–2136.

(33) Crawford, D.; Casaban, J.; Haydon, R.; Giri, N.; Mcnally, T.; James, S. L. Synthesis by extrusion: continuous, large-scale preparation of MOFs using little or no solvent. *Chem. Sci.* **2015**, *6*, 1645–1649.

(34) Karadeniz, B.; Howarth, A. J.; Stolar, T.; Islamoglu, T.; Dejanović, I.; Tireli, M.; Wasson, M. C.; Moon, S.-Y.; Farha, O. K.; Friščić, T.; Užarević, K. Benign by Design: Green and Scalable Synthesis of Zirconium UiO-MetalOrganic Frameworks by Water-Assisted Mechanochemistry. *ACS Sustainable Chem. Eng.* **2018**, *6*, 4–12.

(35) Panda, T.; Horike, S.; Hagi, K.; Ogiwara, N.; Kadota, K.; Itakura, T.; Tsujimoto, M.; Kitagawa, S. Mechanical Alloying of Metal–Organic Frameworks. *Angew. Chem. Int. Ed.* **2017**, *56*, 2413–2417.

(36) Lee, J.-S. M.; Fujiwara, Y.-I.; Kitagawa, S.; Horike, S. Homogenized Bimetallic Catalysts from Metal–Organic Framework Alloys. *Chem. Mater.* **2019**, *31*, 4205–4212.

(37) Andreeva, A. B.; Le, K. N.; Chen, L.; Kellman, M. E.; Hendon, C. H.; Brozek, C. K. Soft Mode Metal-Linker Dynamics in Carboxylate MOFs Evidenced by Variable-Temperature Infrared Spectroscopy. *J. Am. Chem. Soc* **2020**, *142*, 19291–19299, DOI: 10.1021/jacs.0c09499.

(38) Bennett, T. D.; Todorova, T. K.; Baxter, E. F.; Reid, D. G.; Gervais, C.; Bueken, B.; Voorde, B. V. D.; Vos, D. D.; Keen, A.; Mellot-Draznieks, C. Connecting defects and amorphization in UiO-66 and MIL-140 metal–organic frameworks: a combined experimental and computational study. *Phys. Chem. Chem. Phys* **2016**, *18*, 2192–2201.

(39) Mali, G.; Mazaj, M.; Arčon, I.; Hanžel, D.; Arčon, D.; Jagličić, Z. Unraveling the Arrangement of Al and Fe within the Framework Explains the Magnetism of Mixed-Metal MIL-100(Al,Fe). *J. Phys. Chem. Lett.* **2019**, *10*, 1464–1470.

(40) Brunner, E.; Rauche, M. Solid-state NMR spectroscopy: An advancing tool to analyse structure and properties of metal-organic frameworks. *Chem. Sci.* **2020**,

(41) van den Berg, R.; Prieto, G.; Korpershoek, G.; van der Wal, L. I.; van Bunningen, A. J.; Lægsgaard-Jørgensen, S.; de Jongh, P. E.; de Jong, K. P. Structure sensitivity of Cu and CuZn catalysts relevant to industrial methanol synthesis. *Nat. Commun* **2016**, *7*, 13057.

(42) Karelovic, A.; Galdames, G.; Medina, J. C.; Yévenes, C.; Barra, Y.; Jiménez, R. Mechanism and structure sensitivity of methanol synthesis from CO_2 over SiO_2-supported Cu nanoparticles. *J. Catal* **2019**, *369*, 415 – 426.

(43) Graaf, G.; Scholtens, H.; Stamhuis, E.; Beenackers, A. Intra-particle diffusion limitations in low-pressure methanol synthesis. *Chem. Eng. Sci.* **1990**, *45*, 773 – 783.

(44) Froment, G.; Bischoff, K.; De Wilde, J. *Chemical Reactor Analysis and Design, 3rd Edition*; John Wiley & Sons, Inc., 2010.

(45) Yoshihara, J.; Campbell, C. T. Methanol Synthesis and Reverse Water–Gas Shift Kinetics over Cu(110) Model Catalysts: Structural Sensitivity. *J. Catal* **1996**, *161*, 776 – 782.

(46) Morley, C. Gaseq v. 0.79. **2005**, www.gaseq.co.uk (accessed on 1.5.2019.).

(47) Kuld, S.; Thorhauge, M.; Falsig, H.; Elkjær, C. F.; Helveg, S.; Chorkendorff, I.; Sehested, J. Quantifying the promotion of Cu catalysts by ZnO for methanol synthesis. *Science* **2016**, *352*, 969–974.

Graphical TOC Entry